

Modern Physics Letters A
 © World Scientific Publishing Company

PROBING HIGGS-SECTOR CP VIOLATION AT A PHOTON COLLIDER

JAE SIK LEE

*Center for Theoretical Physics, School of Physics and Astronomy,
 Seoul National University, Seoul 151-747, Korea
 jslee@muon.kaist.ac.kr*

In this review we demonstrate physics potential of a photon linear collider by studying the neutral Higgs-boson sector of the MSSM in which interesting CP-violating Higgs mixing could arise via radiative corrections.

Keywords: Higgs; CP violation; Photon collider.

PACS Nos.: 14.80.Cp, 12.60.Jv, 11.30.Er

1. Introduction

The two-photon collision option of the International Linear e^+e^- Collider (ILC), a photon linear collider (PLC), is using back-scattered laser photons off the incident electrons and/or positrons.^{1,2} A photon collider provides unique capabilities for probing new physics appearing in neutral spin-zero particles such as neutral Higgs bosons in the Standard Model (SM) and its Minimal Supersymmetric extension, MSSM.³ The fact that the two-photon energy can reach about 80 % of the e^+e^- center-of-mass (c.m.) energy and the two-photon luminosity can be comparable to or even larger than that of e^+e^- collisions makes it easy to produce Higgs bosons copiously as s -channels resonances at the PLC. Especially, a capability of controlling polarizations of the colliding photons makes the PLC an ideal machine to probe CP properties of the Higgs bosons. In this review, to demonstrate physics potential of the PLC, we investigate the neutral Higgs-boson sector of the MSSM in which CP-violating mixing among scalar and pseudo-scalar states could be radiatively induced.

This review is organized as follows. Section 2 describes a basic mechanism of generating polarized back-scattered laser photons at the ILC. We explicitly show the helicity-dependent $\gamma\gamma$ luminosity as well as the mean polarization of two colliding photon beams. In Sec. 3, we briefly review the Higgs-sector CP violation in the MSSM induced by the CP-violating phases of the soft SUSY breaking terms. Section 4 and Section 5 are devoted to CP violation in s -channel production of Higgs bosons and in the process $\gamma\gamma \rightarrow f\bar{f}$, respectively. Section 6 summarizes our conclusions.

2 Jae Sik Lee

2. A Photon Collider

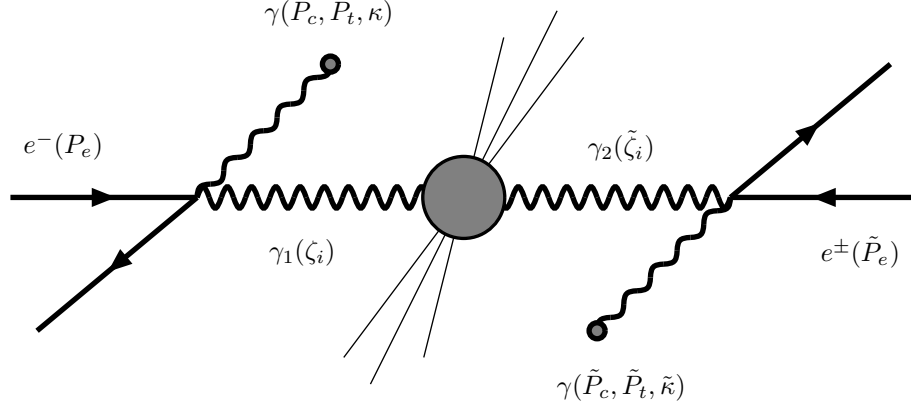


Fig. 1. Schematic diagram of a $\gamma\gamma$ collider. Polarizations of the initial electron and positron beams are denoted by P_e and \tilde{P}_e , respectively. For initial laser photons: P_c and \tilde{P}_c are degrees of circular polarization or mean photon helicity, P_t and \tilde{P}_t the degrees of linear polarization, and κ and $\tilde{\kappa}$ the azimuthal angles of the direction of the maximum linear polarizations. The mean polarizations of the colliding photon beams are denoted by the Stokes parameters ζ_i and $\tilde{\zeta}_i$, see Eq. (8).

The ideal luminosity of the PLC, from the Compton back-scattering of laser photons, is given by ¹

$$\frac{d^2 \mathcal{L}_{\gamma\gamma}}{dy_1 dy_2} = f(y_1) f(y_2) \mathcal{L}_{ee} \quad (1)$$

where

$$y_i \equiv E_{\gamma_i} / E_b \quad (2)$$

with the electron beam energy $E_b = \sqrt{s}/2$. Here s is the invariant ILC energy squared and y_i vary between 0 and $y_{\max} = x/(1+x)$. The machine parameter x depends on E_b and the laser-photon energy ω_0 :

$$x = \frac{4 E_b \omega_0}{m_e^2} = 15.3 \left(\frac{E_b}{\text{TeV}} \right) \left(\frac{\omega_0}{\text{eV}} \right). \quad (3)$$

The function $f(y_1)$ in Eq. (1) is given by

$$f(y_1) = \frac{1}{\sigma_c} \frac{d\sigma_c}{dy_1} = \frac{2\pi\alpha^2}{\sigma_c x m_e^2} [1/(1-y_1) + (1-y_1) - 4r(1-r) - rx(2r-1)(2-y_1)P_e P_c] \quad (4)$$

where

$$r \equiv \frac{y_1}{x(1-y_1)} \rightarrow 1 \text{ as } y_1 \rightarrow y_{\max} \quad (5)$$

and P_e and P_c are polarizations of the initial electron and laser photon beams, respectively, see Fig. 1. For example, $(P_e, P_c) = (+1, +1)$ means the right-handed

electron and laser photon. For a second photon γ_2 , $f(y_2)$ can be obtained by replacing (P_e, P_c) with $(\tilde{P}_e, \tilde{P}_c)$. The total Compton cross-section σ_c in Eq. (4), which is independent of y but depends on the initial electron (positron) and laser-photon polarizations, is given by

$$\begin{aligned}\sigma_c &\equiv \sigma_c^0 + P_e P_c \sigma_c^1, \\ \sigma_c^0 &= \frac{2\pi\alpha^2}{xm_e^2} \left[\left(1 - \frac{4}{x} - \frac{8}{x^2} \right) \log(x+1) + \frac{1}{2} + \frac{8}{x} - \frac{1}{2(x+1)^2} \right], \\ \sigma_c^1 &= \frac{2\pi\alpha^2}{xm_e^2} \left[\left(1 + \frac{2}{x} \right) \log(x+1) - \frac{5}{2} + \frac{1}{x+1} - \frac{1}{2(x+1)^2} \right].\end{aligned}\quad (6)$$

The photon-photon luminosity (1) can be rewritten as

$$\frac{1}{\mathcal{L}_{ee}} \frac{d\mathcal{L}_{\gamma\gamma}}{d\tau} = \int_{\tau/y_{\max}}^{y_{\max}} \frac{dy'}{y'} f(y') f(\tau/y') \quad (7)$$

where $\tau \equiv \hat{s}/s$ with \hat{s} being the c.m. energy of colliding photons γ_1 and γ_2 .

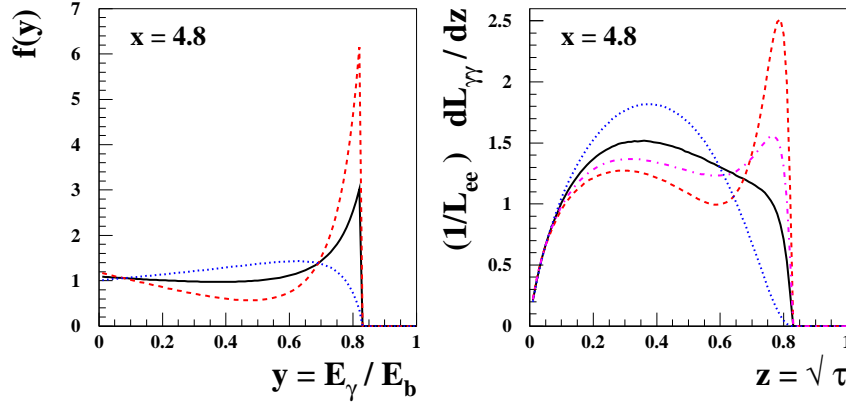


Fig. 2. Photon energy spectrum (left frame) and spectral luminosity of $\gamma\gamma$ collisions (right frame). In the left frame, the solid black line is for $P_e \cdot P_c = 0$, the dashed red line for $P_e \cdot P_c = -1$, and the dotted blue line for $P_e \cdot P_c = 1$. In the right frame, $(P_e \cdot P_c, \tilde{P}_e \cdot \tilde{P}_c) = (0, 0)$, $(-1, -1)$, $(1, 1)$, and $(0, -1)$ for the solid black, dashed red, dotted blue, and dash-dotted magenta lines, respectively.

In Fig. 2, we show $f(y)$ as a function of $y = E_\gamma/E_b$ and $\frac{1}{\mathcal{L}_{ee}} \frac{d\mathcal{L}_{\gamma\gamma}}{dz}$ as a function of $z \equiv \sqrt{\tau}$ for various combinations of initial polarizations $P_e \cdot P_c$ and $\tilde{P}_e \cdot \tilde{P}_c$ taking $x = 4.8$. Note that the functions with $P_e \cdot P_c = \tilde{P}_e \cdot \tilde{P}_c = -1$ (dashed lines) have peaks in the hard photon region.

The polarization of the colliding photon beam is given by the Stokes parameters ζ_i ($\tilde{\zeta}_i$) which describe polarization transfer from the initial laser light and electron (positron) to the colliding photon: ζ_2 is the degree of circular polarization and (ζ_3, ζ_1) are the degrees of linear polarization transverse and normal to the plane defined by the electron direction and the direction of the maximal linear polarization

4 *Jae Sik Lee*

of the initial laser light. The mean polarization is given by

$$\zeta_i = \frac{C_i}{C_0} \quad (8)$$

where, explicitly,

$$\begin{aligned} C_0 &= \frac{1}{1-y} + 1 - y - 4r(1-r) - rx(2r-1)(2-y)P_e P_c = \left(\frac{2\pi\alpha^2}{\sigma_c x m_e^2} \right)^{-1} f(y) \\ C_1 &= 2r^2 P_t \sin 2\kappa \\ C_2 &= rx[(1 + (1-y)(2r-1)^2]P_e - (2r-1)\left(\frac{1}{1-y} + 1 - y\right)P_c \\ C_3 &= 2r^2 P_t \cos 2\kappa \end{aligned} \quad (9)$$

where P_c , P_t , and κ are for the polarization states of the laser photon. Similar relations can be obtained for $\tilde{\zeta}_i$ by replacing (P_c, P_t, κ) with $(\tilde{P}_c, \tilde{P}_t, -\tilde{\kappa})$, see Fig. 1.

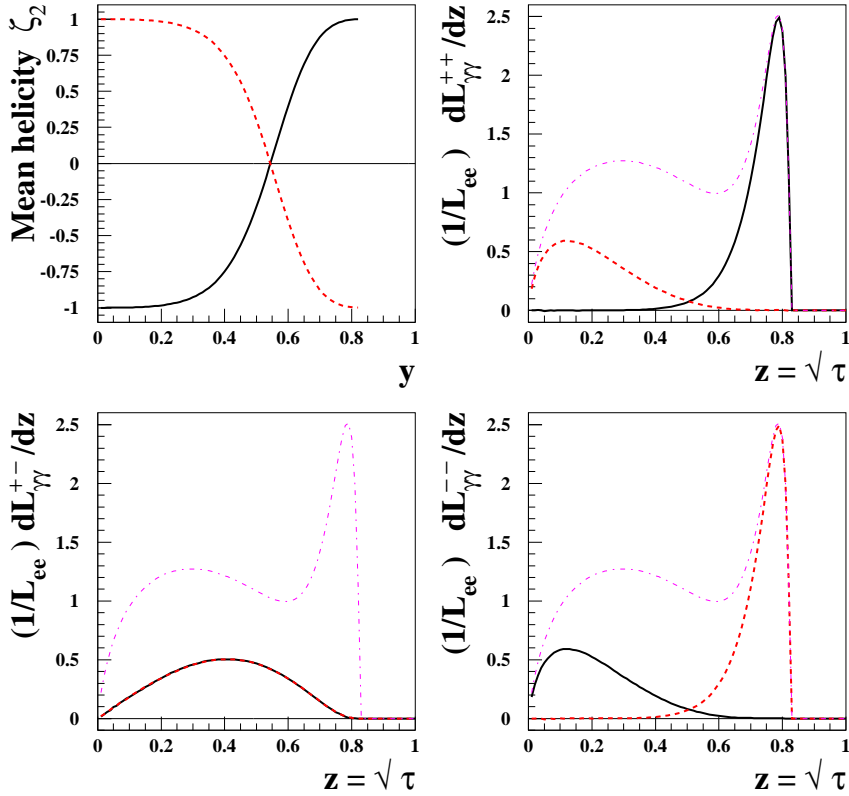


Fig. 3. The mean helicity of the colliding photon beam ζ_2 and the $\gamma\gamma$ luminosity functions $(1/L_{ee}) d\mathcal{L}^{\lambda_1\lambda_2}/dz$ when $P_e \cdot P_c = \tilde{P}_e \cdot \tilde{P}_c = -1$ and $x = 4.8$. The upper indices of the luminosity functions denote the helicity combinations of the colliding photon beams. The solid (black) and dashed (red) lines are for $P_e = \tilde{P}_e = +1$ and -1 . The thin dash-dotted (magenta) lines are for the unpolarized luminosity given by Eq. (7) or $(1/L_{ee}) \sum_{\lambda_1, \lambda_2 = \pm} d\mathcal{L}^{\lambda_1\lambda_2}/dz$.

The mean helicity of the colliding photon beam ζ_2 and the $\gamma\gamma$ luminosity functions for four combinations of helicities are shown in Fig. 3 when $P_e \cdot P_c = \tilde{P}_e \cdot \tilde{P}_c = -1$ taking $x = 4.8$. The $\gamma\gamma$ luminosity function for the helicity combination (λ_1, λ_2) is given by

$$\frac{1}{\mathcal{L}_{ee}} \frac{d\mathcal{L}^{\lambda_1\lambda_2}}{d\sqrt{\tau}} = \left(\frac{\langle 00 \rangle_\tau + \lambda_1 \langle 20 \rangle_\tau + \lambda_2 \langle 02 \rangle_\tau + \lambda_1 \lambda_2 \langle 22 \rangle_\tau}{4} \right) \left(\frac{2\pi\alpha^2}{\sigma_c^{\gamma_1} x m_e^2} \right) \left(\frac{2\pi\alpha^2}{\sigma_c^{\gamma_2} x m_e^2} \right) \quad (10)$$

where $\sigma_c^{\gamma_i}$ is the Compton scattering cross-section given in Eq. (6) and the polarization-correlation is defined as

$$\langle ij \rangle_\tau \equiv 2\sqrt{\tau} \int_{\tau/y_{\max}}^{y_{\max}} \frac{dy'}{y'} C_i(y') C_j(\tau/y'). \quad (11)$$

From Fig. 3, we observe that the mean helicity of a colliding photon is the same as that of the electron at high energy in this case, i.e. $P_e \cdot P_c = \tilde{P}_e \cdot \tilde{P}_c = -1$. Also note that the luminosity functions for $(\lambda_1, \lambda_2) = (\pm, \pm)$ have peaks at high z when $P_e = \tilde{P}_e = \pm$, see the solid (dashed) line in the upper-right (lower-right) frame of Fig. 3.

3. CP Violation in the MSSM Higgs Sector

Any phenomenologically viable SUSY model requires *soft* SUSY breaking terms which break SUSY without spoiling the SUSY resolution to the hierarchy problem. There are three types of soft SUSY breaking terms appearing in the MSSM:

- Gaugino mass terms:

$$\frac{1}{2} \left(M_3 \tilde{g}^a \tilde{g}^a + M_2 \tilde{W}^i \tilde{W}^i + M_1 \tilde{B} \tilde{B} + \text{h.c.} \right), \quad (12)$$

where M_3 is a gluino mass parameter of the gauge group $\text{SU}(3)_c$ and M_2 and M_1 are wino and bino mass parameters of the gauge groups $\text{SU}(2)_L$ and $\text{U}(1)_Y$, respectively.

- Trilinear A terms:

$$\tilde{u}_R^* h_u A_u \tilde{Q} H_2 - \tilde{d}_R^* h_d A_d \tilde{Q} H_1 - \tilde{e}_R^* h_e A_e \tilde{L} H_1 + \text{h.c.}, \quad (13)$$

where \tilde{Q} and \tilde{L} are $\text{SU}(2)_L$ doublet squark and slepton fields and \tilde{u}_R , \tilde{d}_R , and \tilde{e}_R are $\text{SU}(2)_L$ singlet fields.

- Scalar mass terms:

$$\begin{aligned} & \tilde{Q}^\dagger M_Q^2 \tilde{Q} + \tilde{L}^\dagger M_L^2 \tilde{L} + \tilde{u}_R^* M_u^2 \tilde{u}_R + \tilde{d}_R^* M_d^2 \tilde{d}_R + \tilde{e}_R^* M_e^2 \tilde{e}_R \\ & + m_2^2 H_2^* H_2 + m_1^2 H_1^* H_1 - (m_{12}^2 H_1 H_2 + \text{h.c.}). \end{aligned} \quad (14)$$

One crucial observation is that all the massive parameters appearing in the soft SUSY breaking terms can be complex containing nontrivial CP-violating phases. Together with the phase of the Higgsino mass parameter μ of the term $-\mu H_1 H_2$

6 *Jae Sik Lee*

in the superpotential, all the physical observables depend on the CP phases of the combinations $\text{Arg}[M_i \mu (m_{12}^2)^*]$ and $\text{Arg}[A_f \mu (m_{12}^2)^*]$.^{4,5 a}

An interesting phenomenological result of the CP-violating phases is that loop effects mediated dominantly by third-generation squarks with large Yukawa couplings may lead to sizeable violation of the tree-level CP invariance of the MSSM Higgs potential, giving rise to significant Higgs scalar–pseudoscalar transitions.^{6,7,8} The size of the CP-violating mixing is proportional to

$$\frac{3}{16\pi^2} \frac{\Im(A_f \mu)}{m_{\tilde{f}_2}^2 - m_{\tilde{f}_1}^2} \quad (15)$$

with $f = t, b$. At two-loop level, the gluino mass parameter becomes relevant, for example, through the possibly important threshold corrections to the top- and bottom-quark Yukawa couplings.

One consequence of the CP-violating mixing among three MSSM neutral Higgs bosons is that the couplings of Higgs bosons to the SM and SUSY particles are significantly modified. Accordingly the loop-induced Higgs boson couplings to two photons, which receive contributions from all types of charged particles, are largely affected. The amplitude for the production process $\gamma\gamma \rightarrow H_i$ can be written as

$$\mathcal{M}_{\gamma\gamma H_i} = -\frac{\alpha \hat{s}}{4\pi v} \left\{ S_i^\gamma(\hat{s}) (\epsilon_{1\perp} \cdot \epsilon_{2\perp}) - P_i^\gamma(\hat{s}) \frac{2}{\hat{s}} \langle \epsilon_1 \epsilon_2 k_1 k_2 \rangle \right\}, \quad (16)$$

where $k_{1,2}$ are the momenta of the two photons with $(k_1 + k_2)^2 = \hat{s}$ and $\epsilon_{1,2}$ the wave vectors of the corresponding photons, $\epsilon_{1\perp}^\mu = \epsilon_1^\mu - 2k_1^\mu(k_2 \cdot \epsilon_1)/\hat{s}$, $\epsilon_{2\perp}^\mu = \epsilon_2^\mu - 2k_2^\mu(k_1 \cdot \epsilon_2)/\hat{s}$ and $\langle \epsilon_1 \epsilon_2 k_1 k_2 \rangle \equiv \epsilon_{\mu\nu\rho\sigma} \epsilon_1^\mu \epsilon_2^\nu k_1^\rho k_2^\sigma$. The scalar and pseudoscalar form factors, retaining only the dominant loop contributions from the third-generation (s)fermions, charginos, W^\pm and charged Higgs bosons, are given by

$$\begin{aligned} S_i^\gamma(\hat{s}) &= 2 \sum_{f=\tau, b, t, \tilde{\chi}_1^\pm, \tilde{\chi}_2^\pm} N_C Q_f^2 g_f g_{H_i \tilde{f} f}^S \frac{v}{m_f} F_{sf}(\tau_f) \\ &\quad - \sum_{\tilde{f}_j=\tilde{t}_1, \tilde{t}_2, \tilde{b}_1, \tilde{b}_2, \tilde{\tau}_1, \tilde{\tau}_2} N_C Q_{\tilde{f}_j}^2 g_{H_i \tilde{f}_j^* \tilde{f}_j} \frac{v^2}{2m_{\tilde{f}_j}^2} F_0(\tau_{\tilde{f}_j}) \\ &\quad - g_{H_i VV} F_1(\tau_W) - g_{H_i H^+ H^-} \frac{v^2}{2M_{H^\pm}^2} F_0(\tau_{H^\pm}), \\ P_i^\gamma(\hat{s}) &= 2 \sum_{f=\tau, b, t, \tilde{\chi}_1^\pm, \tilde{\chi}_2^\pm} N_C Q_f^2 g_f g_{H_i \tilde{f} f}^P \frac{v}{m_f} F_{pf}(\tau_f), \end{aligned} \quad (17)$$

where $\tau_x = \hat{s}/4m_x^2$, $N_C = 3$ for (s)quarks and $N_C = 1$ for (s)taus and charginos, respectively. For the form factors F_{sf} , F_{pf} , F_0 , and F_1 and the couplings g_f , $g_{H_i \tilde{f} f}^{S,P}$, $g_{H_i VV}$, and $g_{H_i H^+ H^-}$, we refer to Ref. 9.

For numerical examples, we are going to consider two scenarios:

^aIn this review, we are going to take the convention of $\text{Arg}(m_{12}^2) = 0$ while keeping the explicit dependence of $\text{Arg}(\mu)$.

- CPX scenario¹⁰

$$\begin{aligned} M_{\tilde{Q}_3} &= M_{\tilde{U}_3} = M_{\tilde{D}_3} = M_{\tilde{L}_3} = M_{\tilde{E}_3} = M_{\text{SUSY}}, \\ |\mu| &= 4 M_{\text{SUSY}}, \quad |A_{t,b,\tau}| = 2 M_{\text{SUSY}}, \quad |M_3| = 1 \text{ TeV}. \end{aligned} \quad (18)$$

The parameter $\tan\beta$, the charged Higgs-boson pole mass M_{H^\pm} , and the common SUSY scale M_{SUSY} can be varied. For CP phases, taking $\Phi_\mu = 0$ and a common phase $\Phi_A = \Phi_{A_t} = \Phi_{A_b} = \Phi_{A_\tau}$ for A terms, we have two physical phases to vary: Φ_A and $\Phi_3 = \text{Arg}(M_3)$.

- Trimixing scenario^{11 b}

$$\begin{aligned} \tan\beta &= 50, \quad M_{H^\pm} = 155 \text{ GeV}, \\ M_{\tilde{Q}_3} &= M_{\tilde{U}_3} = M_{\tilde{D}_3} = M_{\tilde{L}_3} = M_{\tilde{E}_3} = M_{\text{SUSY}} = 0.5 \text{ TeV}, \\ |\mu| &= 0.5 \text{ TeV}, \quad |A_{t,b,\tau}| = 1 \text{ TeV}, \quad |M_2| = |M_1| = 0.3 \text{ TeV}, \quad |M_3| = 1 \text{ TeV}, \\ \Phi_\mu &= 0^\circ, \quad \Phi_1 = \Phi_2 = 0^\circ, \end{aligned} \quad (19)$$

and we have two varying phases: Φ_A and Φ_3 . In this scenario, all the three-Higgs states mix significantly with their widths larger than the mass differences. For example, for $(\Phi_A, \Phi_3) = (90^\circ, -90^\circ)$, the code `CPsuperH`⁹ generates ^c

$$\begin{aligned} M_{H_1} &= 118.3 \text{ GeV}, \quad M_{H_2} = 119.9 \text{ GeV}, \quad M_{H_3} = 123.6 \text{ GeV}, \\ \Gamma_{H_1} &= 1.27 \text{ GeV}, \quad \Gamma_{H_2} = 7.55 \text{ GeV}, \quad \Gamma_{H_3} = 7.60 \text{ GeV}. \end{aligned} \quad (20)$$

4. CP Violation in s -channel Production of Higgs Bosons

In the two-photon c.m. coordinate system with one photon momentum \mathbf{k}_1 along the positive z direction and the other one \mathbf{k}_2 along the negative z direction, the wave vectors $\epsilon_{1,2}$ of two photons are given by

$$\epsilon_1(\lambda) = \epsilon_2^*(\lambda) = \frac{1}{\sqrt{2}}(0, -\lambda, -i, 0), \quad (21)$$

where $\lambda = \pm 1$ denote the right and left photon helicities, respectively. Inserting the wave vectors into Eq. (16) we obtain the production helicity amplitude for the photon fusion process as follows:

$$\mathcal{M}_{\lambda_1 \lambda_2}^{H_i} = \frac{\alpha M_{H_i}^2}{4\pi v} \{ S_i^\gamma(M_{H_i}^2) + i\lambda_1 P_i^\gamma(M_{H_i}^2) \} \delta_{\lambda_1 \lambda_2}, \quad (22)$$

with $\lambda_{1,2} = \pm 1$, yielding the absolute polarized amplitude squared^{13,14}

$$\overline{|\mathcal{M}^{H_i}|^2} = \overline{|\mathcal{M}^{H_i}|_0^2} \left\{ [1 + \zeta_2 \tilde{\zeta}_2] + \mathcal{A}_1 [\zeta_2 + \tilde{\zeta}_2] + \mathcal{A}_2 [\zeta_1 \tilde{\zeta}_3 + \zeta_3 \tilde{\zeta}_1] - \mathcal{A}_3 [\zeta_1 \tilde{\zeta}_1 - \zeta_3 \tilde{\zeta}_3] \right\}, \quad (23)$$

^bFor an explicit example of the two nearly degenerate heavy Higgs bosons, we refer to Ref. 12.

^cThese values are slightly different from those given in Ref. 11 due to improvements in the calculation of the neutral Higgs-boson pole masses and the treatment of threshold corrections.

8 *Jae Sik Lee*

with the Stokes parameters $\{\zeta_i\}$ and $\{\tilde{\zeta}_i\}$ ($i = 1, 2, 3$) of two photon beams, respectively. The first factor in Eq. (23) is the unpolarized amplitude squared;

$$|\overline{\mathcal{M}^{H_i}}|_0^2 = \frac{1}{4} \left\{ |\mathcal{M}_{++}^{H_i}|^2 + |\mathcal{M}_{--}^{H_i}|^2 \right\} = \frac{1}{2} \left\{ |S_i^\gamma|^2 + |P_i^\gamma|^2 \right\}. \quad (24)$$

and three polarization asymmetries $\mathcal{A}_j^{H_i}$ ($j = 1, 2, 3$) for each H_i are defined in terms of the helicity amplitudes and expressed in terms of the form factors S_i^γ and P_i^γ as

$$\begin{aligned} \mathcal{A}_1^{H_i} &= \frac{|\mathcal{M}_{++}^{H_i}|^2 - |\mathcal{M}_{--}^{H_i}|^2}{|\mathcal{M}_{++}^{H_i}|^2 + |\mathcal{M}_{--}^{H_i}|^2} = \frac{2 \Im(\mathcal{M}_{++}^{H_i} \mathcal{M}_{--}^{H_i*})}{|S_i^\gamma|^2 + |P_i^\gamma|^2}, \\ \mathcal{A}_2^{H_i} &= \frac{2 \Im(\mathcal{M}_{++}^{H_i} \mathcal{M}_{+-}^{H_i*})}{|\mathcal{M}_{++}^{H_i}|^2 + |\mathcal{M}_{--}^{H_i}|^2} = \frac{2 \Re(S_i^\gamma P_i^{\gamma*})}{|S_i^\gamma|^2 + |P_i^\gamma|^2}, \\ \mathcal{A}_3^{H_i} &= \frac{2 \Re(\mathcal{M}_{+-}^{H_i} \mathcal{M}_{++}^{H_i*})}{|\mathcal{M}_{++}^{H_i}|^2 + |\mathcal{M}_{--}^{H_i}|^2} = \frac{|S_i^\gamma|^2 - |P_i^\gamma|^2}{|S_i^\gamma|^2 + |P_i^\gamma|^2}. \end{aligned} \quad (25)$$

In the CP-invariant theories with real couplings, the form factors S_i^γ and P_i^γ cannot exist simultaneously and they should satisfy the relations; $\mathcal{A}_1^{H_i} = \mathcal{A}_2^{H_i} = 0$ and $\mathcal{A}_3^{H_i} = +1(-1)$ depending on whether the Higgs boson is a pure CP-even (CP-odd) state. In other words, $\mathcal{A}_1^{H_i} \neq 0$, $\mathcal{A}_2^{H_i} \neq 0$ and/or $|\mathcal{A}_3^{H_i}| < 1$ ensure that H_i is a mixture of CP-even and CP-odd states, implying CP violation. We note that both circularly and transversely polarized initial laser beams are needed to measure all three polarization asymmetries, see Eqs. (8) and (9). Finally, the s -channel Higgs-boson production $\gamma\gamma \rightarrow H_i$ is given by

$$\sigma(\gamma\gamma \rightarrow H_i) = \hat{\sigma}_0(H_i) \delta(1 - M_{H_i}^2/\hat{s}) = \frac{\alpha^2}{32\pi v^2} (|S_i^\gamma|^2 + |P_i^\gamma|^2) \delta(1 - M_{H_i}^2/\hat{s}), \quad (26)$$

where $\alpha_{\text{em}}^2/32\pi v^2 \sim 4 \text{ fb}$.

In Fig. 4, we show the cross-section $\hat{\sigma}_0(H_i)$ and three polarization asymmetries $\mathcal{A}_{1,2,3}^{H_i}$ as functions of Higgs-boson masses taking the CPX scenario. We observe sizeable effects of CP violation in all three polarization asymmetries except $\mathcal{A}_{1,2,3}^{H_1}$ in the decoupling limit $M_{H^\pm} \gtrsim 200 \text{ GeV}$. Moreover, the polarization asymmetries $\mathcal{A}_1^{H_i}$ and $\mathcal{A}_2^{H_i}$ are complementary in the sense that one asymmetry is large where the other one is small.

5. CP Violation in $\gamma\gamma \rightarrow f\bar{f}$

In this section, we study the processes $\gamma\gamma \rightarrow f\bar{f}$ including the QED continuum background as well as the Higgs contribution.^{15,16,17,18,19}

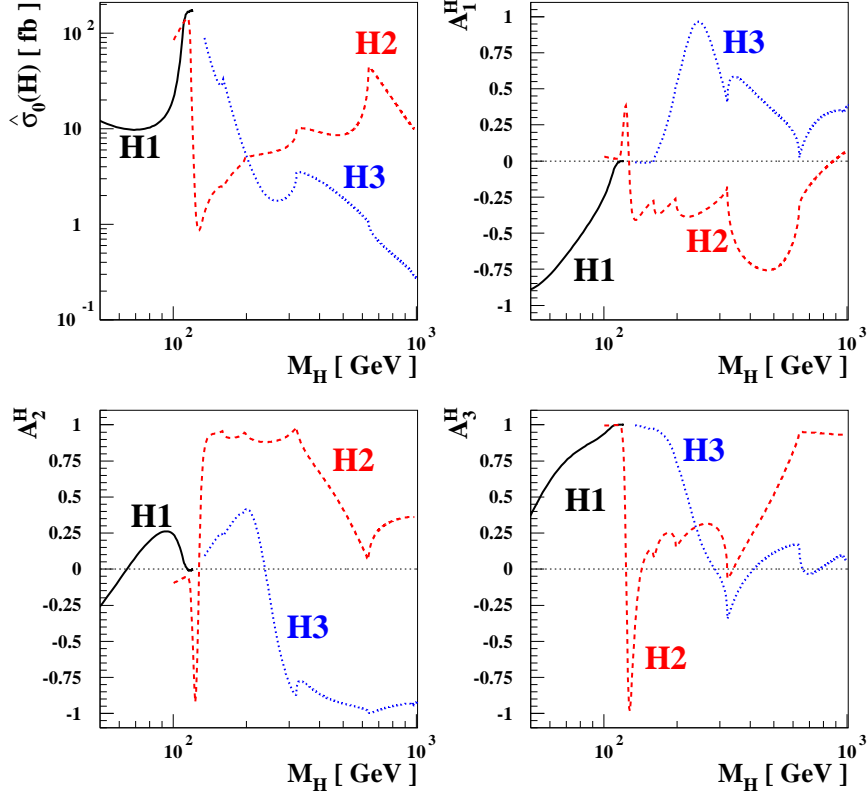


Fig. 4. The parton cross-section $\hat{\sigma}_0(H_i)$ in units of fb and three polarization asymmetries $\mathcal{A}_{1,2,3}^{H_i}$ as functions of each Higgs-boson mass for the CPX scenario taking $\tan \beta = 5$, $M_{\text{SUSY}} = 500$ GeV, and $\Phi_A = \Phi_3 = 90^\circ$.

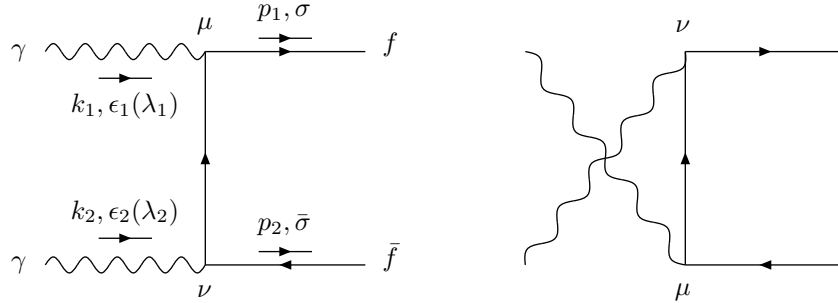


Fig. 5. Feynman diagrams contributing to the tree-level QED background, introducing our definitions of the initial-state photon and final-state fermion momenta and helicities.

5.1. Helicity Amplitudes

The tree-level Feynman diagrams for the QED process $\gamma\gamma \rightarrow \bar{f}f$ are shown in Fig. 5. In the two-photon c.m. system, the helicity amplitudes for the QED production of

10 *Jae Sik Lee*

a fermion-antifermion pair take the forms:

$$\mathcal{M}_C = 4\pi\alpha Q_f^2 \langle \sigma \bar{\sigma}; \lambda_1 \lambda_2 \rangle_C, \quad (27)$$

where

$$\begin{aligned} \langle \sigma \sigma; \lambda \lambda \rangle_C &= \frac{4m_f}{\sqrt{\hat{s}}} \frac{1}{1 - \beta_f^2 c_\theta^2} (\lambda + \sigma \beta_f); & \langle \sigma \sigma; \lambda - \lambda \rangle_C &= -\frac{4m_f}{\sqrt{\hat{s}}} \frac{s_\theta^2}{1 - \beta_f^2 c_\theta^2} \sigma \beta_f; \\ \langle \sigma - \sigma; \lambda \lambda \rangle_C &= 0; & \langle \sigma - \sigma; \lambda - \lambda \rangle_C &= -2\beta_f \frac{s_\theta}{1 - \beta_f^2 c_\theta^2} (\sigma \lambda + c_\theta). \end{aligned} \quad (28)$$

We use the abbreviations $s_\theta \equiv \sin \theta$ and $c_\theta \equiv \cos \theta$ with θ the angle between \mathbf{p}_1 and \mathbf{k}_1 , and $\beta_f \equiv \sqrt{1 - 4m_f^2/\hat{s}}$ with $\hat{s} = (k_1 + k_2)^2 = (p_1 + p_2)^2$. We allow for independent and measurable polarizations $\lambda_{1,2}$ of the initial-state photons and $\bar{\sigma}, \sigma$ of the final-state fermion-antifermion pair. We note that the last amplitude in (28) with completely different helicity states is the least important, since the Higgs-mediated diagram is nonvanishing only when the helicities of photons and/or those of final fermions are equal.

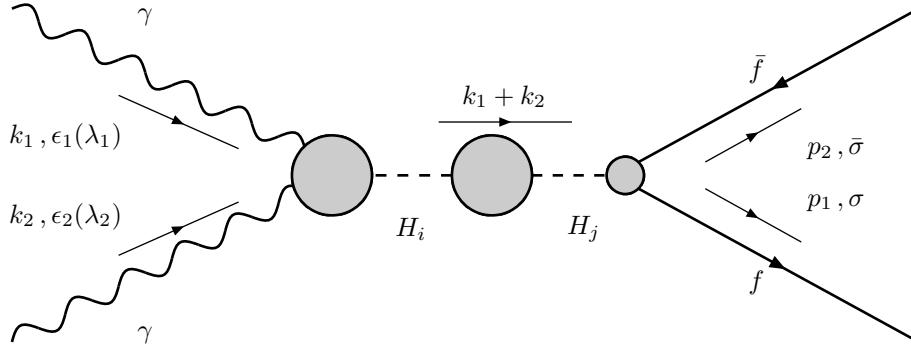


Fig. 6. Mechanisms contributing to the process $\gamma\gamma \rightarrow H_{1,2,3} \rightarrow \bar{f}f$, including off-diagonal absorptive parts in the Higgs-boson propagator matrix.

The helicity amplitudes of the process $\gamma\gamma \rightarrow H \rightarrow \bar{f}f$, see Fig. 6, are given by

$$\mathcal{M}_H = \frac{\alpha m_f \sqrt{\hat{s}}}{4\pi v^2} \langle \sigma; \lambda_1 \rangle_H \delta_{\sigma\bar{\sigma}} \delta_{\lambda_1 \lambda_2}, \quad (29)$$

where the reduced amplitude ^d

$$\langle \sigma; \lambda \rangle_H = - \sum_{i,j=1}^3 [S_i^\gamma(\hat{s}) + i\lambda P_i^\gamma(\hat{s})] D_{ij}(\hat{s}) (\sigma \beta_f g_{H_j \bar{f}f}^S - i g_{H_j \bar{f}f}^P), \quad (30)$$

^dHere we have corrected an error in the overall sign of the amplitude. ¹⁸

is a quantity given by the Higgs-boson propagator matrix $D_{ij}(\hat{s})$ combined with the production and decay vertices. In the calculation of the propagator matrix $D_{ij}(\hat{s})$, we have fully included the off-diagonal absorptive parts which cannot be neglected when two or more MSSM Higgs bosons contribute simultaneously to the process under consideration.^{11,20}

We note the following properties of the $\gamma\gamma \rightarrow \bar{f}f$ helicity amplitudes under the CP transformation:

$$\langle \sigma \bar{\sigma}; \lambda_1 \lambda_2 \rangle \xrightarrow{\text{CP}} (-1)(-1)^{(\sigma-\bar{\sigma})/2} \langle -\bar{\sigma} - \sigma; -\lambda_2 - \lambda_1 \rangle. \quad (31)$$

Also interesting are the properties under the CPT transformation, where $\tilde{\text{T}}$ reverses the signs of the spins and the three-momenta of the asymptotic states, without interchanging initial and final states, and the matrix element gets complex conjugated:

$$\langle \sigma \bar{\sigma}; \lambda_1 \lambda_2 \rangle \xrightarrow{\text{CPT}} (-1)(-1)^{(\sigma-\bar{\sigma})/2} \langle -\bar{\sigma} - \sigma; -\lambda_2 - \lambda_1 \rangle^*. \quad (32)$$

Evidently, the QED helicity amplitudes (28) are even under both the CP and CPT transformations. On the other hand, the simultaneous presence of $\{S_i^\gamma, P_i^\gamma\}$ and/or $\{g_{H_j \bar{f}f}^S, g_{H_j \bar{f}f}^P\}$ would signal CP violation in the Higgs-boson-exchange amplitude (30), and nonvanishing absorptive parts from the vertices and the propagators could also lead to CPT violation in the Higgs-exchange diagram.

5.2. Identical Photon and Fermion Helicities

The most appealing case may be that of identical photon and fermion helicities due to the m_f suppression of the large QED background (28) and the relative easiness in controlling the mean helicities of the colliding photon beams and measuring the longitudinal polarizations of the final fermions. In this case the amplitude may be written as

$$\mathcal{M}_{\sigma\lambda}^{\text{I}} = \mathcal{M}_C|_{\bar{\sigma}=\sigma, \lambda_1=\lambda_2=\lambda} + \mathcal{M}_H = \frac{\alpha m_f \sqrt{\hat{s}}}{4\pi v^2} \langle \sigma; \lambda \rangle \quad (33)$$

where \mathcal{M}_C and \mathcal{M}_H are given in Eqs. (27) and (29), respectively. The amplitude $\langle \sigma; \lambda \rangle$ consists of two terms as

$$\langle \sigma; \lambda \rangle \equiv \langle \sigma; \lambda \rangle_H + R(\hat{s})f(\theta)\langle \sigma; \lambda \rangle_C, \quad (34)$$

where $R(\hat{s}) = 64\pi^2 Q_f^2 v^2 / \hat{s}$, $f(\theta) = 1/(1 - \beta_f^2 c_\theta^2)$, and $\langle \sigma; \lambda \rangle_C = \lambda + \sigma\beta_f$, see Eq. (28). We note that $\langle \sigma = \mp; \lambda = \pm \rangle_C = \pm(1 - \beta_f)$, which vanishes in the limit $m_f \rightarrow 0$.

Depending on the different combinations of helicities of the initial-state photons and final-state fermions, we have four differential cross-sections:

$$\frac{d\hat{\sigma}_{\sigma\lambda}}{dc_\theta} = \frac{\beta_f N_C}{32\pi\hat{s}} |\mathcal{M}_{\sigma\lambda}^{\text{I}}|^2 \quad (35)$$

where $\sigma, \lambda = \pm$. After integrating them over c_θ , we have the cross-sections

$$\hat{\sigma}_{\sigma\lambda} = \frac{\beta_f N_C}{32\pi} \left(\frac{\alpha m_f}{4\pi v^2} \right)^2 \mathcal{Y}_{\sigma\lambda} \quad (36)$$

12 *Jae Sik Lee*

with the \hat{s} -dependent functions

$$\begin{aligned} \mathcal{Y}_{\sigma\lambda} &\equiv \int_{-z_f}^{z_f} dc_\theta |\langle\sigma; \lambda\rangle|^2 \\ &= 2 \left\{ z_f |\langle\sigma; \lambda\rangle_H|^2 + R(\hat{s})^2 F_1^{z_f} |\langle\sigma; \lambda\rangle_C|^2 + R(\hat{s}) F_2^{z_f} \Re [\langle\sigma; \lambda\rangle_H \langle\sigma; \lambda\rangle_C^*] \right\}. \end{aligned} \quad (37)$$

The functions $F_1^{z_f}$ and $F_2^{z_f}$ are given by

$$\begin{aligned} F_1^{z_f} &= \frac{1}{2} \int_{-z_f}^{z_f} dc_\theta f^2(\theta) = \frac{z_f}{2(1 - z_f^2 \beta_f^2)} + \frac{\ln \frac{1+z_f \beta_f}{1-z_f \beta_f}}{4\beta_f}, \\ F_2^{z_f} &= \int_{-z_f}^{z_f} dc_\theta f(\theta) = \frac{\ln \frac{1+z_f \beta_f}{1-z_f \beta_f}}{\beta_f}. \end{aligned} \quad (38)$$

Note that we have introduced an experimental cut on the fermion polar angle θ : $|\cos \theta| \leq z_f$ and $\cos \theta_{\text{cut}}^f = z_f$. Experimentally, we cannot measure the final state fermion if it has too small angle θ outside the coverage of detectors. This angular cut has significant effects in the cases of light fermions, $f = \mu, \tau$, and b , since the QED continuum differential cross-section $d\hat{\sigma}_C/dc_\theta$ is peaked in the forward and backward directions. This makes the cross-section $\hat{\sigma}_C$, or $F_1^{z_f}$, strongly depend on z_f when the final fermions are light:

$$\hat{\sigma}_C \equiv \frac{\beta_f N_C}{16\pi} \left(\frac{\alpha m_f}{4\pi v^2} \right)^2 R(\hat{s})^2 F_1^{z_f} \frac{\sum_{\sigma, \lambda=\pm} |\langle\sigma; \lambda\rangle_C|^2}{4}. \quad (39)$$

Actually the QED cross-sections are suppressed by factors of about 5000 and 20 for $f = \mu$ and $f = \tau$ cases, respectively, by imposing $\theta_{\text{cut}}^{\mu, \tau} = 130$ mrad angle cut ($z_{\mu, \tau} \simeq 0.99$) when $\sqrt{\hat{s}} = 120$ GeV. For b -quark case, the suppression factor is about 30 imposing $\theta_{\text{cut}}^b = 280$ mrad ($z_b \simeq 0.96$). On the other hand, the Higgs-mediated cross-section and the QED continuum cross-section for top quarks are hardly affected by the polar angle cut. The introduction of the polar angle cut, therefore, greatly enhance the significance of the Higgs-mediated process with respect to the QED continuum one for $f = \mu, \tau$, and b .

The CP and CPT parities of the polarization-dependent cross sections $\hat{\sigma}_{\sigma\lambda}$ (36) can easily be obtained by observing that

$$\mathcal{Y}_{\sigma\lambda} \xleftrightarrow{\text{CP}} \mathcal{Y}_{-\sigma-\lambda}, \quad \mathcal{Y}_{\sigma\lambda} \xleftrightarrow{\text{CPT}} \mathcal{Y}_{-\sigma-\lambda}, \quad (40)$$

which are derived from (31) and (32). Based on this observation, we can construct two CP-violating cross-sections in terms of $\hat{\sigma}_{\sigma\lambda}$:

$$\hat{\Delta}_1 \equiv \hat{\sigma}_{++} - \hat{\sigma}_{--}, \quad \hat{\Delta}_2 \equiv \hat{\sigma}_{+-} - \hat{\sigma}_{-+}, \quad (41)$$

or, equivalently, the two linear combinations

$$(\hat{\Delta}_1 + \hat{\Delta}_2) = \sum_{\lambda=\pm} (\hat{\sigma}_{+\lambda} - \hat{\sigma}_{-\lambda}), \quad (\hat{\Delta}_1 - \hat{\Delta}_2) = \sum_{\sigma=\pm} (\hat{\sigma}_{\sigma+} - \hat{\sigma}_{\sigma-}). \quad (42)$$

Note that the CP-violating cross-section ($\hat{\Delta}_1 - \hat{\Delta}_2$) can be determined without measuring the helicities of the final-state fermions. Finally, the unpolarized total cross-section is given by

$$\hat{\sigma}_{\text{tot}} = \frac{1}{4} (\hat{\sigma}_{++} + \hat{\sigma}_{--} + \hat{\sigma}_{+-} + \hat{\sigma}_{-+}) . \quad (43)$$

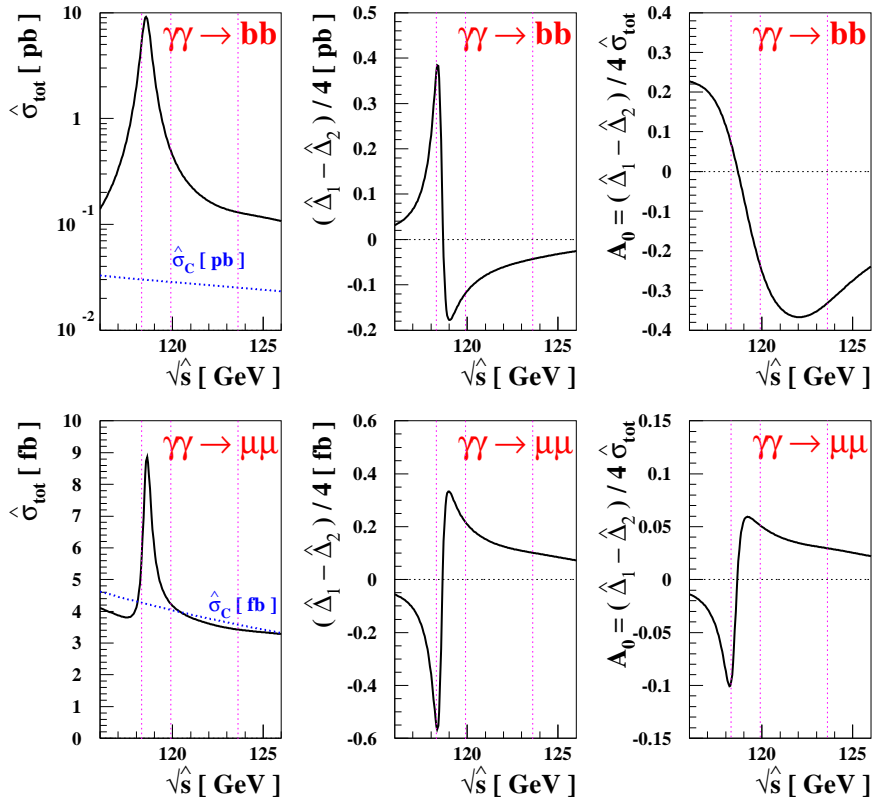


Fig. 7. The cross-sections $\hat{\sigma}_{\text{tot}}$ and $(\hat{\Delta}_1 - \hat{\Delta}_2)/4$ and the CP asymmetry \mathcal{A}_0 as functions of $\sqrt{\hat{s}}$ for the processes $\gamma\gamma \rightarrow b\bar{b}$ (upper frames) and $\gamma\gamma \rightarrow \mu^+\mu^-$ (lower frames) in the trimixing scenario with $(\Phi_A, \Phi_3) = (90^\circ, -90^\circ)$. The continuum cross-sections $\hat{\sigma}_C$ are also shown in the left frames as dotted lines. The three Higgs masses are indicated by vertical lines.

First we consider the processes $\gamma\gamma \rightarrow b\bar{b}$ and $\gamma\gamma \rightarrow \mu^+\mu^-$ in which the helicities of the final-state fermions cannot be measured. In Fig. 7, we show the cross-sections $\hat{\sigma}_{\text{tot}}$ and $(\hat{\Delta}_1 - \hat{\Delta}_2)/4$ and the CP asymmetry \mathcal{A}_0 defined by

$$\mathcal{A}_0 \equiv \frac{\hat{\Delta}_1 - \hat{\Delta}_2}{4 \hat{\sigma}_{\text{tot}}} . \quad (44)$$

Assuming an integrated $\gamma\gamma$ luminosity of 100 fb^{-1} , and high efficiency for b -quark reconstruction, we may expect more than ten thousand events with the total cross-section larger than $\sim 0.1 \text{ pb}$ in the process $\gamma\gamma \rightarrow b\bar{b}$. This would enable one to

probe CP asymmetry at the 1 % level or less. For the process $\gamma\gamma \rightarrow \mu^+\mu^-$ we expect to have a few hundred events with a 100 fb^{-1} integrated $\gamma\gamma$ luminosity. The CP asymmetry \mathcal{A}_0 can be probed only when it is larger than a few %. But, differently from the $\gamma\gamma \rightarrow \bar{b}b$ process, the good resolution in the muon invariant mass enables us to examine the \sqrt{s} dependence of the cross-sections and the CP asymmetry.

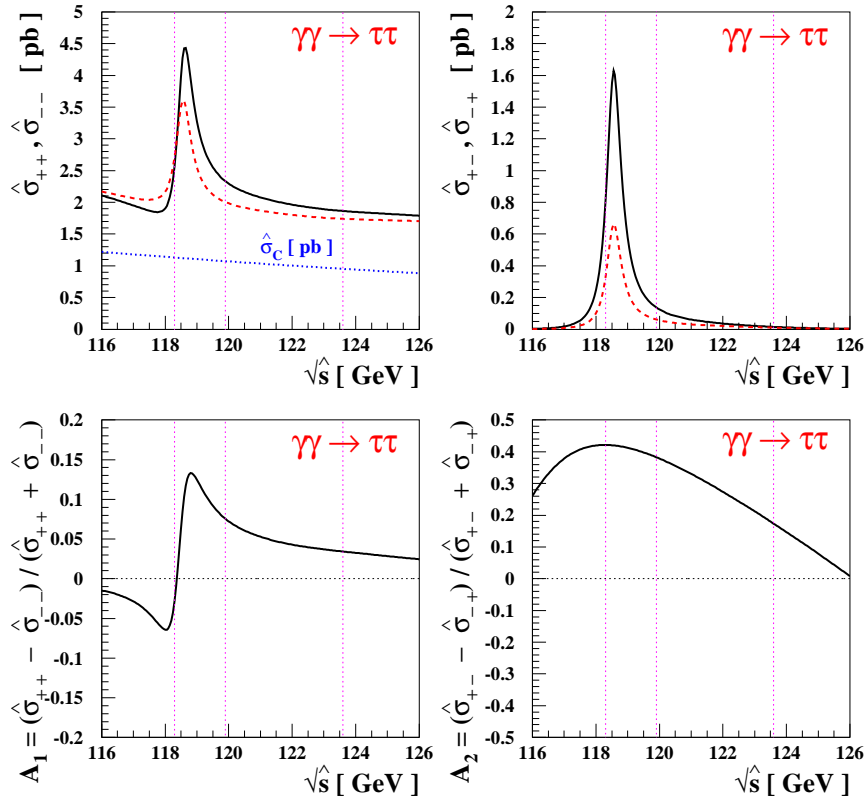


Fig. 8. The cross-sections $\hat{\sigma}_{\sigma\lambda}$ (upper frames) and the CP asymmetries $\mathcal{A}_{1,2}$ (lower frames) as functions of \sqrt{s} for the processes $\gamma\gamma \rightarrow \tau^+\tau^-$ in the trimixing scenario with $(\Phi_A, \Phi_3) = (90^\circ, -90^\circ)$. The solid lines are for $\hat{\sigma}_{++}$ and $\hat{\sigma}_{+-}$ and the dashed lines for $\hat{\sigma}_{--}$ and $\hat{\sigma}_{-+}$ in the upper two frames. The continuum cross-section $\hat{\sigma}_C$ is also shown in the upper-left frame as a dotted line. The three Higgs masses are indicated by vertical lines.

In the process $\gamma\gamma \rightarrow \tau^+\tau^-$, the polarizations of final tau leptons can be measured through its decays. In Fig. 8, we show the cross-sections $\hat{\sigma}_{\sigma\lambda}$ in (36) in the upper frames. When $\sigma = \lambda$ (upper-left frame), the cross-sections are around 2-4 pb and we observe the sizable difference between $\hat{\sigma}_{++}$ (solid) and $\hat{\sigma}_{--}$ (dashed), which is just the $\hat{\Delta}_1$. When $\sigma \neq \lambda$ (upper-right frame), the cross-sections are peaked between M_{H_1} and M_{H_2} with their sizes of about 1.6 pb ($\hat{\sigma}_{+-}$) and 0.6 pb ($\hat{\sigma}_{-+}$) as shown by solid and dashed lines, respectively. Again we see a sizable difference between

the two cross-sections, which is the CP-violating cross-section $\hat{\Delta}_2$. One may define two CP-odd asymmetries as:

$$\mathcal{A}_1 \equiv \frac{\hat{\Delta}_1}{\hat{\sigma}_{++} + \hat{\sigma}_{--}}, \quad \mathcal{A}_2 \equiv \frac{\hat{\Delta}_2}{\hat{\sigma}_{+-} + \hat{\sigma}_{-+}}. \quad (45)$$

Assuming 10,000 $\gamma\gamma \rightarrow \tau^+\tau^-$ events after applying some experimental cuts to reconstruct the tau leptons and their polarizations, CP-odd asymmetries larger than 1 % could be measured.

5.3. Initial and Final Spin-spin Correlations

The polarizations of the final fermions can be measured in the processes such as $\gamma\gamma \rightarrow \tau^+\tau^-$, $t\bar{t}$, $\chi_i^+\chi_j^-$, $\chi_i^0\chi_j^0$, etc. In this case, one can construct a lot of observables through initial and final spin-spin correlations. It is convenient to consider two cases separately: (i) identical fermion helicities, $\sigma = \bar{\sigma}$ and (ii) identical photon helicities, $\lambda = \lambda_1 = \lambda_2$.

5.3.1. Identical fermion helicities: initial photon spin-spin correlations

In this case, for each σ , the amplitude can be cast into a 2×2 matrix:

$$(\mathcal{M}_\sigma^{\text{II}})_{\lambda_1\lambda_2} = \frac{\alpha m_f \sqrt{\hat{s}}}{4\pi v^2} \begin{pmatrix} \langle\sigma; +\rangle & \langle\sigma\rangle_C \\ \langle\sigma\rangle_C & \langle\sigma; -\rangle \end{pmatrix} \quad \text{with} \quad \langle\sigma\rangle_C \equiv -R(\hat{s}) s_\theta^2 f(\theta) \sigma \beta_f, \quad (46)$$

and the $\langle\sigma; \lambda\rangle$ defined in (34). With the polarization density matrices for the two photons:

$$\tilde{\rho} = \frac{1}{2} \begin{pmatrix} 1 + \tilde{\zeta}_2 & -\tilde{\zeta}_3 + i\tilde{\zeta}_1 \\ -\tilde{\zeta}_3 - i\tilde{\zeta}_1 & 1 - \tilde{\zeta}_2 \end{pmatrix}, \quad \rho = \frac{1}{2} \begin{pmatrix} 1 + \zeta_2 & -\zeta_3 + i\zeta_1 \\ -\zeta_3 - i\zeta_1 & 1 - \zeta_2 \end{pmatrix}, \quad (47)$$

the polarization-weighted squared matrix elements can be obtained by ²¹

$$|\mathcal{M}_\sigma^{\text{II}}|^2 = \text{Tr} [\mathcal{M}_\sigma^{\text{II}} \tilde{\rho} \mathcal{M}_\sigma^{\text{II}\dagger} \rho^T]. \quad (48)$$

The amplitude squared for each σ can be expanded as

$$|\mathcal{M}_\sigma^{\text{II}}|^2 = \left(\frac{\alpha m_f \sqrt{\hat{s}}}{4\pi v^2} \right)^2 \left\{ A_1^\sigma (1 + \zeta_2 \tilde{\zeta}_2) + A_2^\sigma [(\zeta_1 \tilde{\zeta}_1 - \zeta_2 \tilde{\zeta}_2) + (\zeta_3 \tilde{\zeta}_3 - \zeta_2 \tilde{\zeta}_2)] \right. \\ \left. + B_1^\sigma (\zeta_2 + \tilde{\zeta}_2) + B_2^\sigma (\zeta_1 \tilde{\zeta}_3 + \zeta_3 \tilde{\zeta}_1) + B_3^\sigma (\zeta_3 \tilde{\zeta}_3 - \zeta_1 \tilde{\zeta}_1) \right. \\ \left. + C_1^\sigma (\zeta_1 + \tilde{\zeta}_1) + C_2^\sigma (\zeta_3 + \tilde{\zeta}_3) + C_3^\sigma (\zeta_1 \tilde{\zeta}_2 + \zeta_2 \tilde{\zeta}_1) + C_4^\sigma (\zeta_2 \tilde{\zeta}_3 + \zeta_3 \tilde{\zeta}_2) \right\},$$

where the polarization coefficients are given by

$$\begin{aligned}
A_1^\sigma &= \frac{1}{4} (|\langle\sigma; +\rangle|^2 + |\langle\sigma; -\rangle|^2 + 2|\langle\sigma\rangle_C|^2) ; \quad A_2^\sigma = \frac{1}{2} |\langle\sigma\rangle_C|^2, \\
B_1^\sigma &= \frac{1}{4} (|\langle\sigma; +\rangle|^2 - |\langle\sigma; -\rangle|^2) ; \quad B_2^\sigma = \frac{1}{2} \Im[\langle\sigma; +\rangle \langle\sigma; -\rangle^*] ; \\
B_3^\sigma &= \frac{1}{2} \Re[\langle\sigma; +\rangle \langle\sigma; -\rangle^*] , \\
C_1^\sigma &= -\frac{1}{2} \Im[(\langle\sigma; +\rangle - \langle\sigma; -\rangle) \langle\sigma\rangle_C^*] ; \quad C_2^\sigma = -\frac{1}{2} \Re[(\langle\sigma; +\rangle + \langle\sigma; -\rangle) \langle\sigma\rangle_C^*] ; \\
C_3^\sigma &= -\frac{1}{2} \Im[(\langle\sigma; +\rangle + \langle\sigma; -\rangle) \langle\sigma\rangle_C^*] ; \quad C_4^\sigma = -\frac{1}{2} \Re[(\langle\sigma; +\rangle - \langle\sigma; -\rangle) \langle\sigma\rangle_C^*] . \quad (49)
\end{aligned}$$

We note that $B_{2,3}^\sigma$ are related to the observables in the interference between the amplitudes with different photon helicities requiring linear polarizations of the colliding photon beams, and that the observables C_i^σ are due to interference with the QED continuum.

5.3.2. Identical photon helicities: final fermion spin-spin correlations

In this case, for each λ , the amplitude can be cast into a diagonal 2×2 matrix:

$$(\mathcal{M}_\lambda^{\text{III}})_{\sigma\bar{\sigma}} = \frac{\alpha m_f \sqrt{\hat{s}}}{4\pi v^2} \begin{pmatrix} \langle +; \lambda \rangle & 0 \\ 0 & \langle -; \lambda \rangle \end{pmatrix} , \quad (50)$$

where $\langle \pm; \lambda \rangle$ are defined in (34). The polarization density matrices for the two final-state fermions are

$$\bar{\rho} = \frac{1}{2} \begin{pmatrix} 1 + \bar{P}_L & -\bar{P}_T e^{i\bar{\alpha}} \\ -\bar{P}_T e^{-i\bar{\alpha}} & 1 - \bar{P}_L \end{pmatrix} , \quad \rho = \frac{1}{2} \begin{pmatrix} 1 + P_L & P_T e^{-i\alpha} \\ P_T e^{i\alpha} & 1 - P_L \end{pmatrix} . \quad (51)$$

Here, P_L and \bar{P}_L are the longitudinal polarizations of the fermion f and antifermion \bar{f} , respectively, while P_T and \bar{P}_T are the degrees of transverse polarization with α and $\bar{\alpha}$ being the azimuthal angles with respect to the production plane. For each λ , the polarization-weighted squared matrix elements are ²¹

$$\begin{aligned}
|\mathcal{M}_\lambda^{\text{III}}|^2 &= \text{Tr} [\mathcal{M}_\lambda^{\text{III}} \bar{\rho}^T \mathcal{M}_\lambda^{\text{III}\dagger} \rho] = \left(\frac{\alpha m_f \sqrt{\hat{s}}}{4\pi v^2} \right)^2 \left\{ D_1^\lambda (1 + P_L \bar{P}_L) + D_2^\lambda (P_L + \bar{P}_L) \right. \\
&\quad \left. + P_T \bar{P}_T [D_3^\lambda \cos(\alpha - \bar{\alpha}) + D_4^\lambda \sin(\alpha - \bar{\alpha})] \right\} , \quad (52)
\end{aligned}$$

where

$$\begin{aligned}
D_1^\lambda &= \frac{1}{4} (|\langle +; \lambda \rangle|^2 + |\langle -; \lambda \rangle|^2) ; \quad D_2^\lambda = \frac{1}{4} (|\langle +; \lambda \rangle|^2 - |\langle -; \lambda \rangle|^2) ; \\
D_3^\lambda &= -\frac{1}{2} \Re(\langle +; \lambda \rangle \langle -; \lambda \rangle^*) ; \quad D_4^\lambda = \frac{1}{2} \Im(\langle +; \lambda \rangle \langle -; \lambda \rangle^*) . \quad (53)
\end{aligned}$$

The quantities $D_{3,4}^\lambda$ are related to the observables coming from the interference between the amplitudes with different fermion helicities, for which we need to determine the transverse polarizations of the final fermions.

5.3.3. Observables

We consider two categories of cross-sections, according to the final-state fermion helicity σ or the initial-state photon helicity λ :

$$\begin{aligned}\frac{d\hat{\Sigma}^X}{dc_\theta} &\equiv \frac{\beta_f N_C}{32\pi} \left(\frac{\alpha m_f}{4\pi v^2} \right)^2 (X^+ + X^-), \\ \frac{d\hat{\Delta}^X}{dc_\theta} &\equiv \frac{\beta_f N_C}{32\pi} \left(\frac{\alpha m_f}{4\pi v^2} \right)^2 (X^+ - X^-),\end{aligned}\tag{54}$$

where $X^\pm = A_i^\sigma, B_j^\sigma, C_k^\sigma, D_l^\lambda$. In this way, we can construct more than 20 independent observables. It can be shown that half of the observables are CP-odd using Eqs. (31) and (32), see Table 1. We refer to Ref. 18 for some numerical examples of the observables $\hat{\Sigma}^X$ and $\hat{\Delta}^X$ in the processes $\gamma\gamma \rightarrow \tau^+\tau^-$ and $\gamma\gamma \rightarrow t\bar{t}$.

Table 1. The CP and CPT parities of the cross-sections.

A type [CP, CPT]	B type [CP, CPT]	C type [CP, CPT]	D type [CP, CPT]
$\hat{\Sigma}^{A_1}[+, +]$	$\hat{\Sigma}^{B_1}[-, -]$	$\hat{\Sigma}^{C_1}[-, +]$	$\hat{\Sigma}^{D_1}[+, +]$
$\hat{\Sigma}^{A_2}[+, +]$	$\hat{\Sigma}^{B_2}[-, +]$	$\hat{\Sigma}^{C_2}[+, +]$	$\hat{\Sigma}^{D_2}[-, -]$
	$\hat{\Sigma}^{B_3}[+, +]$	$\hat{\Sigma}^{C_3}[+, -]$	$\hat{\Sigma}^{D_3}[+, +]$
		$\hat{\Sigma}^{C_4}[-, -]$	$\hat{\Sigma}^{D_4}[-, +]$
$\hat{\Delta}^{A_1}[-, -]$	$\hat{\Delta}^{B_1}[+, +]$	$\hat{\Delta}^{C_1}[+, -]$	$\hat{\Delta}^{D_1}[-, -]$
$\hat{\Delta}^{A_2}[-, -]$	$\hat{\Delta}^{B_2}[+, -]$	$\hat{\Delta}^{C_2}[-, -]$	$\hat{\Delta}^{D_2}[+, +]$
	$\hat{\Delta}^{B_3}[-, -]$	$\hat{\Delta}^{C_3}[-, +]$	$\hat{\Delta}^{D_3}[-, -]$
		$\hat{\Delta}^{C_4}[+, +]$	$\hat{\Delta}^{D_4}[+, -]$

6. Conclusions

The capability of controlling polarizations of the colliding photons makes the PLC an ideal machine for probing CP properties of neutral spin-zero particles. To illustrate this capability, we have investigated the neutral Higgs-boson sector of the MSSM in which interesting CP-violating mixing could arise via radiative corrections. First we have considered CP violation in inclusive s -channel Higgs production and constructed three asymmetries $\mathcal{A}_{1,2,3}^{H_i}$ for each H_i . And we have presented a general formalism for analyzing CP-violating phenomena in the process $\gamma\gamma \rightarrow \bar{f}f$ by exploiting controllable beam polarizations and possibly measurable final-fermion polarizations. We have shown that one can construct more than 20 independent observables for each decay mode and half of them are CP-odd.

Acknowledgments

I wish to thank E. Asakawa, S.Y. Choi, K. Hagiwara, J. Ellis, and A. Pilaftsis for valuable collaborations. In particular, I would like to thank S.Y. Choi for careful reading of the manuscript. This work was supported in part by the Korea Research

Foundation (KRF) and the Korean Federation of Science and Technology Societies Grant and in part by the KRF grant KRF-2005-084-C00001 funded by the Korea Government (MOEHRD, Basic Research Promotion Fund).

References

1. I. F. Ginzburg, G. L. Kotkin, S. L. Panfil, V. G. Serbo and V. I. Telnov, Nucl. Instrum. Meth. A **219** (1984) 5.
2. B. Badelek *et al.* [ECFA/DESY Photon Collider Working Group], Int. J. Mod. Phys. A **19** (2004) 5097 [arXiv:hep-ex/0108012].
3. See, for example, K. Hagiwara, Nucl. Instrum. Meth. A **472** (2001) 12 [arXiv:hep-ph/0011360].
4. M. Dugan, B. Grinstein and L. J. Hall, Nucl. Phys. B **255** (1985) 413.
5. S. Dimopoulos and S. D. Thomas, Nucl. Phys. B **465** (1996) 23 [arXiv:hep-ph/9510220].
6. A. Pilaftsis, Phys. Rev. D **58** (1998) 096010 [arXiv:hep-ph/9803297].
7. A. Pilaftsis, Phys. Lett. B **435** (1998) 88 [arXiv:hep-ph/9805373].
8. See references in E. Accomando *et al.*, arXiv:hep-ph/0608079.
9. J. S. Lee, A. Pilaftsis, M. Carena, S. Y. Choi, M. Drees, J. R. Ellis and C. E. M. Wagner, Comput. Phys. Commun. **156** (2004) 283 [arXiv:hep-ph/0307377].
10. M. Carena, J. R. Ellis, A. Pilaftsis and C. E. M. Wagner, Phys. Lett. B **495** (2000) 155 [arXiv:hep-ph/0009212].
11. J. R. Ellis, J. S. Lee and A. Pilaftsis, Phys. Rev. D **70** (2004) 075010 [arXiv:hep-ph/0404167].
12. S. Y. Choi, J. Kalinowski, Y. Liao and P. M. Zerwas, Eur. Phys. J. C **40** (2005) 555 [arXiv:hep-ph/0407347].
13. B. Grzadkowski and J. F. Gunion, Phys. Lett. B **294** (1992) 361 [arXiv:hep-ph/9206262].
14. S. Y. Choi and J. S. Lee, Phys. Rev. D **62** (2000) 036005 [arXiv:hep-ph/9912330].
15. E. Asakawa, J. i. Kamoshita, A. Sugamoto and I. Watanabe, Eur. Phys. J. C **14** (2000) 335 [arXiv:hep-ph/9912373].
16. E. Asakawa, S. Y. Choi, K. Hagiwara and J. S. Lee, Phys. Rev. D **62** (2000) 115005 [arXiv:hep-ph/0005313].
17. R. M. Godbole, S. D. Rindani and R. K. Singh, Phys. Rev. D **67** (2003) 095009 [Erratum-ibid. D **71** (2005) 039902] [arXiv:hep-ph/0211136].
18. J. R. Ellis, J. S. Lee and A. Pilaftsis, Nucl. Phys. B **718** (2005) 247 [arXiv:hep-ph/0411379].
19. R. M. Godbole, S. Kraml, S. D. Rindani and R. K. Singh, Phys. Rev. D **74** (2006) 095006 [Erratum-ibid. D **74** (2006) 119901] [arXiv:hep-ph/0609113].
20. J. S. Lee, arXiv:hep-ph/0409020.
21. K. Hagiwara and D. Zeppenfeld, Nucl. Phys. B **274** (1986) 1.